Long-term rail profile damage in a railway crossing: Field measurements and numerical simulations

Citation for the original published paper (version of record):
Skrypnyk, R., Ossberger, U., Pålsson, B. et al (2021). Long-term rail profile damage in a railway crossing: Field measurements and numerical simulations. Wear, 472-473. http://dx.doi.org/10.1016/j.wear.2020.203331

Wear 472-473 (2021) 203331

Contents lists available at ScienceDirect

Wear

journal homepage: http://www.elsevier.com/locate/wear

Long-term rail profile damage in a railway crossing: Field measurements and numerical simulations

Rostyslav Skrypnyk [a,*], Uwe Ossberger [b], Björn A. Pålsson [a], Magnus Ekh [c], Jens C.O. Nielsen [a]

[a] Department of Mechanics and Maritime Sciences/CHARMEC, Chalmers University of Technology, SE-412 96, Gothenburg, Sweden
[b] Voestalpine VAE GmbH, Zeltweg, Austria
[c] Department of Industrial and Materials Science/CHARMEC, Chalmers University of Technology, SE-412 96, Gothenburg, Sweden

ARTICLE INFO

Keywords:
Dynamic vehicle–track interaction
Switches & crossings
S&C
FEM
Plastic deformation
Wear

ABSTRACT

Railway crossings are subjected to a severe load environment leading to a degradation of rail profiles due to wear and accumulated plastic deformation. This damage is the result of the high magnitudes of contact pressure and traction generated in the wheel–rail contact during each wheel transition between wing rail and crossing nose. An extensive measurement campaign has been carried out at a test site in Austria in a particularly severely loaded crossing manufactured from an explosion depth hardened (EDH) manganese steel grade. For an accumulated traffic load of 65 Mega-Gross-Tonnes (MGT), the evolution of profile degradation for 16 cross-sections along the crossing rail has been recorded on multiple occasions. The results from the measurement campaign are used to validate a previously presented multidisciplinary and iterative simulation methodology for the prediction of long-term rail damage. It is shown that the predicted rail profile degradation exceeds the measured degradation for some of the cross-sections but generally a good qualitative agreement is observed. Possible reasons for the higher predicted damage are the uncertain distribution of traffic at the test site and differences in material properties between the crossing in the field and the test specimens used for calibration of the cyclic plasticity model. The influence of the frequency of updating the rail profiles in the iterative simulation methodology, and the compromise between computational cost and the number of load cases accounted for in the applied load sequence, are addressed.

1. Introduction

Railway turnouts (switches and crossings, S&C) are an integral part of a railway network providing flexibility by connecting different tracks. This flexibility, however, comes at a considerable cost due to the needs for maintenance and replacement of switch rails and crossings. The conventional turnout design with a fixed crossing introduces a change in rail profile leading to variations in wheel–rail contact geometry (see e.g. Ref. [1,2]). The dynamic wheel–rail interaction in the crossing panel, including the high impact load induced by the dip angle in the vertical wheel trajectory at the transition between wing rail and crossing nose, leads to material deterioration of the crossing by traffic in both facing and trailing directions (moves) [3].

For a given traffic scenario, several approaches can be considered to reduce the material damage in a crossing. One is to optimise the geometry of the crossing nose and wing rails to provide a smoother wheel trajectory, see e.g. Ref. [4]. Another is to optimise the dynamic properties of the resilient elements in the crossing, e.g. the stiffness of rail pads, base plate pads and under sleeper pads. This approach was explored in Ref. [5], where it was demonstrated that the magnitude of the impact load is more influenced by deviations from the nominal wheel–rail contact geometry than by the selection of rail pad stiffness. The approach this study relies on is the possibility to select the rail material such that the long-term damage in the crossing is minimised. In previous work [6], a simulation methodology has been proposed that, for a given traffic situation, allows for a critical assessment of the long-term performance of different rail materials. The methodology has previously been validated by comparing predicted rail profiles with those measured in the field at Härad (switch rail) in Sweden [6] and Haste (crossing rail) in Germany [7].

Three damage mechanisms have been identified as the most detrimental to the life of a crossing nose. These are accumulated plastic deformation, wear and rolling contact fatigue (RCF). Only the former two are addressed in the present study. Plastic deformation arises due to

* Corresponding author.
E-mail address: rostyslav.skrypnyk@chalmers.se (R. Skrypnyk).

https://doi.org/10.1016/j.wear.2020.203331
Received 21 January 2020; Received in revised form 1 April 2020; Accepted 30 April 2020
Available online 23 June 2020

micromechanical processes in the grain structure of the material and leads to a permanent shape change of the rail. Explicit finite element (FE) simulations of wheel and crossing contact are often used to compute the plastic deformation of a crossing due to the dynamic vehicle–track interaction. This approach was adopted in Ref. [8], where it was shown that the highest short-term plastic deformation occurred in the crossing nose, independent of the simulated traffic move. However, such simulations are computationally very expensive, which prohibits their use in the assessment of long-term damage.

Wear is removal of material from a contact surface and is, therefore, associated with the change of volume of the material. A recent study [9], accounting for wear and plastic deformation, suggests that the maximum values of both plastic deformation and frictional work occur at positions of two-point contact during the transition between the rails, and not at the position of maximum normal contact force. Two situations that induce wear were identified in Ref. [10]: sliding and rolling. The relative motion tangential to the surface (sliding) has a larger potential for causing wear than the orthogonal motion (impact and rolling). Sliding occurs in the slip region of the wheel–rail contact patch due to the tangential relative motion between the wheel and rail surfaces.

The multidisciplinary and iterative methodology presented in Ref. [6] may consider all of these three damage mechanisms. It may also take into account the variability in traffic conditions, such as the influence of different wheel profiles interacting with the rails, the variation in friction coefficient in the wheel–rail contact and different vehicle speeds. The iterative methodology consists of four steps: (I) Simulation of dynamic vehicle–track interaction; (II) Analysis of wheel–rail normal contact; (III) Prediction of accumulated rail damage; (IV) Updating of rail profiles, which are then used as input in the next iteration of the methodology.

It is well established, see e.g. Refs. [11], that accounting for plasticity plays a significant role in wheel–rail contact analysis. Recently, the contact simulation in step II of this methodology has been enhanced with a Hertzian-based metamodel [12] that was calibrated against FE simulations using an elasto-plastic material model. This makes it possible to reduce the computational cost of the methodology associated with the large number of three-dimensional and physically nonlinear FE analyses of wheel–rail contact that needs to be carried out for a representative load sequence. In Ref. [13], the methodology was demonstrated by comparing the plastic deformation and wear for one cross-section of the crossing nose for two different materials. For a prescribed number of load cycles, corresponding to an accumulated traffic load of 0.8 MGT, it was concluded that the fine-pearlitic rail grade R350HT experienced half of the ratchetting displacement compared with the austenitic hot-rolled manganese steel Mn13.

The aim of the present work is to further validate the methodology by comparing predictions with measured data in terms of plastic deformation and wear for an increased accumulated traffic load, as well as refining it in terms of robustness and efficiency.

2. Field tests

Over a period of five years, corresponding to an accumulated traffic load of 65 MGT, a series of rail profile measurements in an explosion depth hardened (EDH) manganese steel crossing in Zeltweg (Austria) has been performed by voestalpine VAE GmbH. The measured crossing is subjected to a particularly severe load environment as it is in a curved turnout located in a transition curve with curve radius in the through route varying between 592 and 932 m, as well as cant varying between 0 and 70 mm.

The turnout is exposed to mixed traffic with maximum vehicle speed 90 km/h in the through route. The distribution of traffic is estimated to be 90% in the through route and 10% in the diverging route. However, information about the distribution of traffic in facing and trailing moves was not available. The axle load for the passenger trains varied between 14 and 18 tonnes (only in locomotives the axle load was 22.5 tonnes).

On 12 occasions over the period of five years (see Fig. 1), the profiles of 16 cross-sections of the crossing rail have been measured using the non-contact profile measurement device CALIPRI. The accuracy of each measurement sample is ±80 μm. A possible source of error is a potential longitudinal misalignment of the equipment by a few millimetres between repeated measurements of the same cross-section. The initial measurement (0 MGT) was done after milling and after all burrs had been manually removed. Fig. 1 shows the change of the crossing nose height over time. It was obtained from the measured height difference between the wing rail, at a reference position (for each cross-section) not affected by damage, and the crossing nose. It is observed that the installed crossing had a profile height that exceeded the design given by the drawing.

A characteristic feature of the manganese steel used in railway crossings is a relatively low yield limit combined with a rather low hardening modulus and high ductility. This means that a significant plastic deformation occurs during the initial cycles, which enables the crossing to adapt its shape to the load environment. Owing to this property, the frequency of measurements was chosen to be gradually decreasing from once a month at the beginning to once every half year at the end of the measurement campaign. The small downward slope between 700 and 900 mm that can be observed in the initial measurements, see Fig. 1, is an artefact stemming from the wing rail not having the same height in this region. It is observed that the slope of the crossing in the transition region was continuously increasing throughout the measurement period in the absence of maintenance work.

An assembly of a set of measurements performed for the 16 cross-sections, see the horizontal lines in Fig. 2, shows which parts of the crossing are subjected to the severest loading. For each data point on the initial cross-section, the normal distance to the corresponding damaged profile was calculated. This procedure was repeated for every measured cross-section. The values in-between the cross-sections were obtained by linear interpolation. The colours represent the distance between the virgin profile and the damaged profile in the direction normal to the initial surface. The positive direction is inwards. The negative values represent relocated material. A significant change of rail profile is observed for the crossing nose and the gauge corner of the wing rails.

An example of profile evolution over time is presented in Fig. 3. A comparison of a given profile measured on different occasions makes it possible to distinguish between plastic deformation and wear. The wear area A_w is chosen to be computed as the difference between the initial area A_0 of the cross-section and the current area A:

$$A_w = A_0 - A \tag{1}$$

This allows to introduce a measure of the shape change (plastic deformation) area A_u as the integral over the profile width of the absolute surface vertical displacement $\underline{u}_z$ (relative to the initial geometry) excluding the wear area:

$$A_u = \int |\underline{u}_z(y)|\, dy - A_w \tag{2}$$

Based on the repeated measurements, it is possible to visualise the history of different damage mechanisms along the crossing rail, see Fig. 4. Fig. 4(a) shows the time history of wear area of the measured cross-sections, where each grid intersection corresponds to a measurement. It is observed that, initially, wear peaked at three cross-sections, approximately at 250, 400 and 650 mm after the tip of the crossing. The second peak has become inconspicuous over time. Fig. 4(b) presents the time history of shape change area. It shows that the crossing rail has been subjected to severe plastic deformation in the region between 300 and 400 mm. The corresponding rates of wear area and shape change area are shown in Fig. 4(c) and (d). Note that the plastic deformation was the dominating damage mechanism in the beginning, but after about 25–30 MGT it was taken over by wear.

A more detailed picture of the first 12 MGT of traffic is shown in Fig. 5. The observed occasional decrease of damage for several cross-

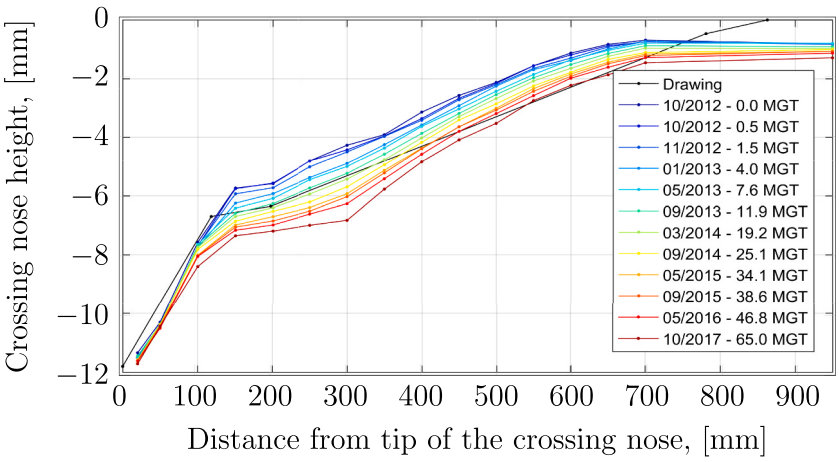

Fig. 1. Evolution of crossing nose height measured using the top of the wing rail as reference.

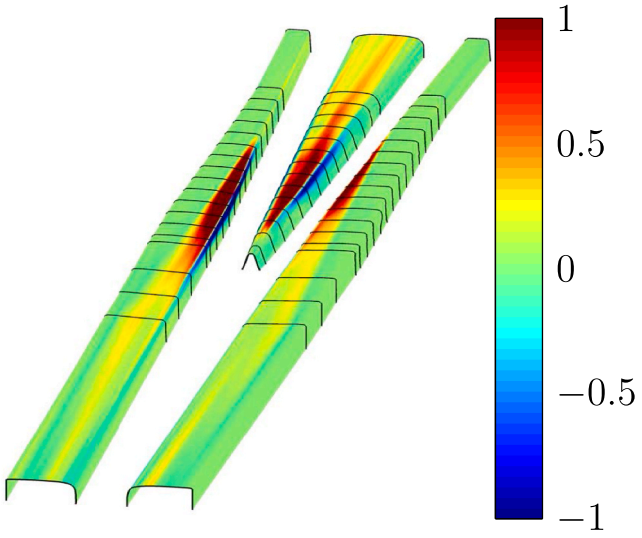

Fig. 2. Measured geometry change of surface [mm] after 19.2 MGT.

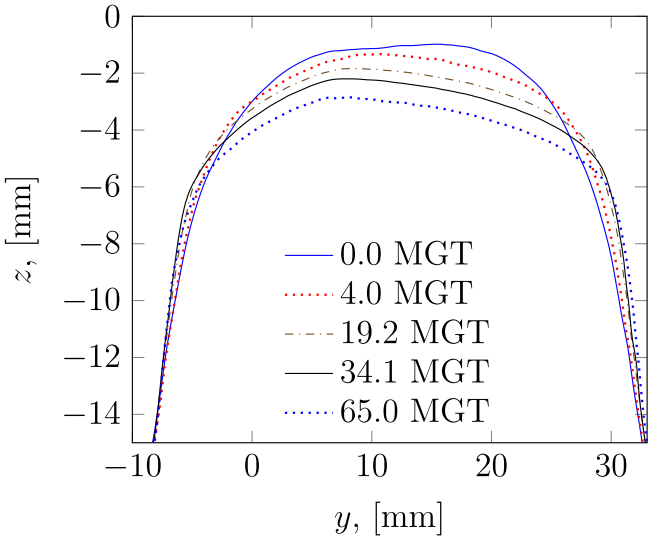

Fig. 3. Measured evolution of rail profile at cross-section 350 mm after the tip of the crossing. The profiles were aligned in the lateral direction based on a reference point at $z = -20$ mm, which is far away from any wheel–rail contact.

sections indicates a possible measurement error due to longitudinal misalignment of CALIPRI. Apart from the initial set of measurements (up to 1.5 MGT), in Fig. 5(c) it is observed that the wear rate has been close to constant. The high initial wear rate could be due to a different (abrasive) wear mechanism and higher contact stresses in the new crossing rail during the first load cycles. Unlike the wear rate, the rate of plastic deformation remained nearly constant for the first 12 MGT, see Fig. 5(d). It can also be observed that the plastic deformation has spanned a shorter section of the crossing rail compared with the wear.

For each measured rail profile and when evaluated over all recorded measurements, the largest observed increase in cross-section area between two subsequent measurements is summarised in Table 1. Such an increase in area is non-physical and the maximum observed value can therefore be interpreted as an indication of the error in measurement data. The maximum value of 6 mm^2 was observed for the cross-section located 400 mm after the tip of the crossing. Therefore, it can be argued that the uncertainty in Fig. 4(a) and (b), 5(a) and 5(b) is ± 6 mm^2.

3. Simulation methodology

The multidisciplinary and iterative methodology to predict the long-term degradation of rail profiles due to mixed traffic conditions has been presented and extended in previous papers, see Ref. [6,7,13]. Starting from a set of nominal rail profiles with virgin material, the methodology to predict the degradation of rail profiles in a crossing consists of simulations of dynamic vehicle–track interaction, wheel–rail normal contact and accumulated damage (in this paper, plastic deformation and wear; see Fig. 6). In this study, the applied load sequence includes N_1 identical vehicles (each with N_{axle} axles) with N_1 different wheel profiles. A load collective is generated by repeating the load sequence N_2 times. Fig. 7 illustrates the assembly of a load collective consisting of N_2 identical load sequences, where each sequence includes $N_{\text{axle}} \cdot N_1$ load cycles. The accumulated degradation of the rails due to plastic deformation and wear is calculated considering the applied load collective. Then, the rail profiles are updated and the methodology is repeated N_3 times in a simulation loop until the required accumulated traffic load has been simulated.

The model for simulation of dynamic vehicle–track interaction has been developed in the multibody simulation (MBS) software Simpack. It includes the Manchester benchmarks passenger vehicle model [14] and a model of the turnout representing the conditions at the test site in Austria. The model uses the Hertzian method for normal contact and the FASTSIM algorithm [15] for the tangential contact. For wheel–rail contact at the top of a crossing rail, it was shown in Ref. [11] that the Hertzian contact model provides sufficient accuracy at low cost compared with two non-elliptical models: Kalker's variational method

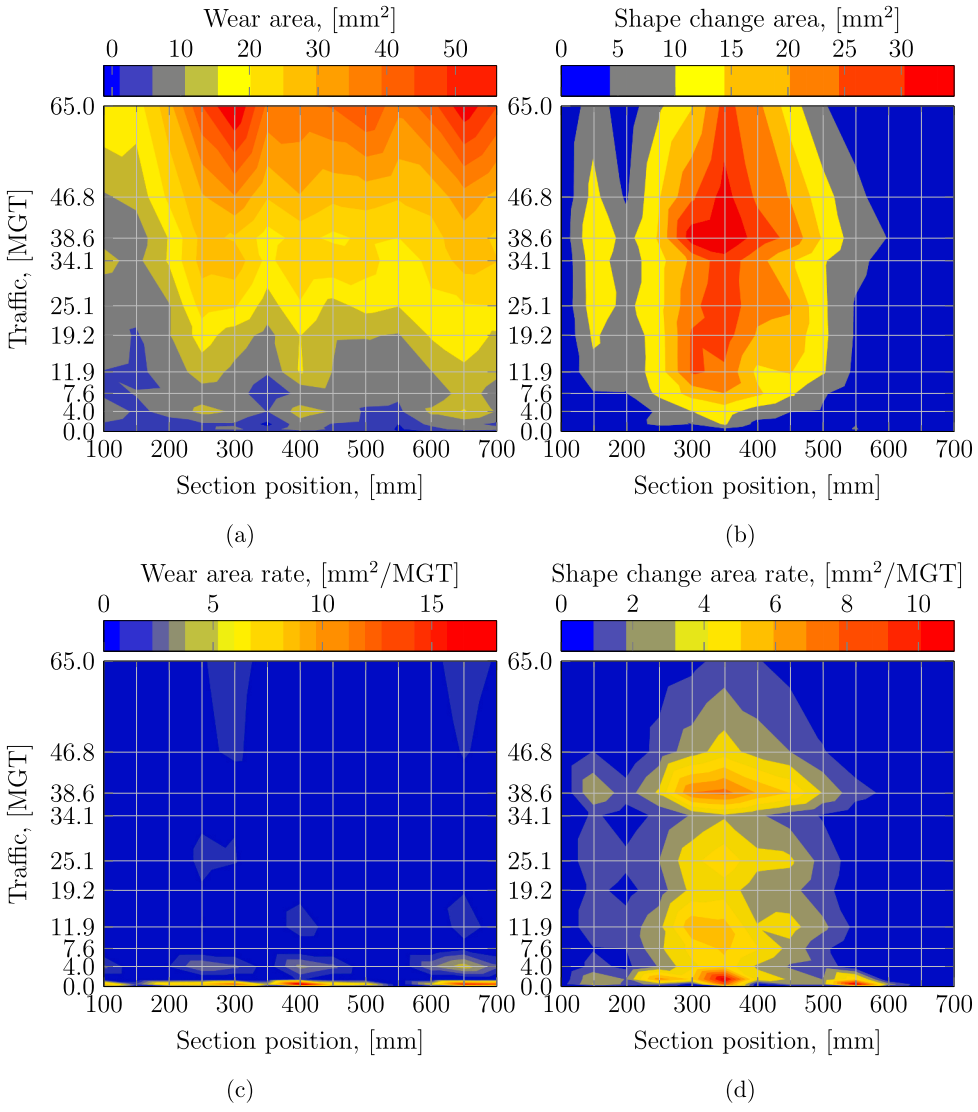

Fig. 4. Measurement data over time and length of the crossing for different damage measures: (a) wear area, [mm^2], (b) shape change area, [mm^2] (c) wear area rate, [mm^2/MGT] and (d) shape change area rate, [mm^2/MGT].

and FEM. The output from each simulation are the time histories of the magnitudes and locations of the normal and tangential wheel–rail contact forces (and creepages) used for computing the damage. Even though the high-frequency contribution to the contact forces cannot be captured accurately using MBS [16], it can be approximated with a proper choice of track model. The model from Ref. [17] was employed in this study. The "TM2" configuration (nine degrees of freedom) of co-running track model with a system of rigid masses, springs and dampers following each wheelset is used (see Ref. [17] for more details). The model was calibrated to measured track receptance data up to 200 Hz.

In the present study, it was found that the full vehicle model with carbody and two bogies can be replaced by a simpler vehicle model consisting of only one bogie. This is because, for the relevant responses within the methodology (such as contact point location and force magnitude), the difference between the two models was acceptable, see Fig. 8. The lateral contact point position curves of the reduced model overlap with the corresponding curves on the wing and the crossing rail of both the front and rear bogies of the full model. The observed difference in the contact force is due to the missing coupling between the front and rear bogies via the car body for a vehicle passing through a transition curve with changing superelevation (see Section 2).

Vehicle speed, wheel–rail friction coefficient and wheel profile are examples of important input parameters in the simulations of damage and degradation of rail profiles as they affect the location of contact positions and magnitude of the wheel–rail contact forces. To account for the varying traffic conditions that a crossing would experience in the field, the applied load sequence should mimic the variation in these parameters. This can be achieved using a sample of N_1 measured wheel profiles to represent the variation in wheel profile geometry, while certain probability distributions can be assumed for vehicle speed and wheel–rail friction coefficient. Using the Latin Hypercube Sampling (LHS) technique (see e.g. Ref. [18]), N_1 unique random combinations (load cases) of these three parameters for simulations of vehicle–track interaction can be constructed.

Elliptic contact is assumed in the contact step of the methodology (see Ref. [12] for a discussion of the validity of such an approach in S&Cs). The assumed simplified geometry reduces the computational cost significantly due to the reduced size of the symmetric FE model. It also made it possible to use a Hertzian-based metamodel that provides an additional reduction of the computational effort compared with a full FE model, while still being able to account for plastic response.

The simulation of damage includes calculations of accumulated plastic deformation and sliding wear. The plastic deformation is computed with an in-house FE code using 2D plane strain assumption for

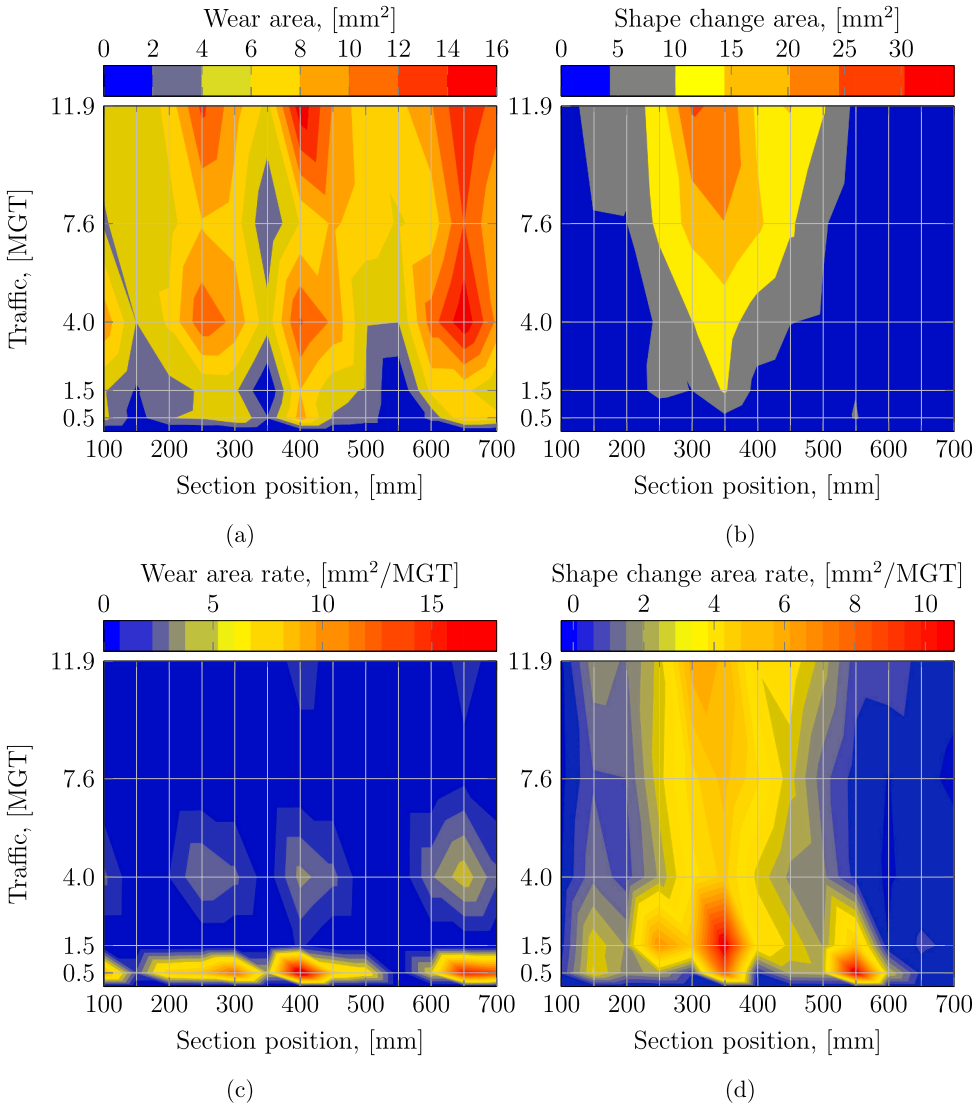

Fig. 5. Zoom-in to initial measurement data over time and length of the crossing for different damage measures: (a) wear area, [mm^2], (b) shape change area, [mm^2], (c) wear area rate, [mm^2/MGT] and (d) shape change area rate, [mm^2/MGT].

Table 1
Maximum observed increase in profile area (mm^2) between two subsequent measurements for all cross-sections in the transition region (between 100 and 700 mm). Boldface denotes maximum value.

Section	100	150	200	250	300	350	400	450	500	550	600	650	700
Area	5.77	1.53	1.02	3.65	3.93	3.35	**6.18**	5.24	1.11	0.48	4.31	3.54	2.92

each of the selected rail cross-sections and a cyclic plasticity model of Ohno-Wang type [19] with three back stresses (see Ref. [13] for more details). It was calibrated against uniaxial stress-controlled ratchetting experimental data for hot-rolled manganese steel, which has different behaviour than the EDH manganese steel. The principal difference between the two materials is that the latter one has a higher yield limit near the surface, which gradually drops with increasing distance from the surface. Such characteristics are difficult to reproduce in the test specimens used in laboratory experiments. This is why, in this study the yield limit σ_y in the material model was modified to the average yield limit of the EDH steel reported by the crossing manufacturer, $\sigma_y = 580$ MPa.

Kalker's model FASTSIM [15] and Archard's wear model [20] are used to carry out the wear simulations. The input data (contact position, contact force and creepages) for the prediction of wear are provided by the simulation of dynamic vehicle–track interaction using the MBS software (see Ref. [13] for more details on the wear prediction model). The material parameters for the wear model could be extracted from a seldom available wear map (see e.g. Ref. [21]). Since no wear map was available for the pair of wheel and rail materials considered in the present study, the wear model was first calibrated against the measured average wear rate after 4 MGT. However, when accounting also for plasticity, this resulted in a worse agreement with the measured crossing geometry in terms of total damage compared to the case when it was calibrated against the average wear rate of 140 mm^3/MGT for another EDH manganese crossing in Nicklasdorf (Austria) (see Ref. [13]). This is due to the fact that the calculations of plasticity rely on the model, calibrated for a material that has lower hardening modulus than the one

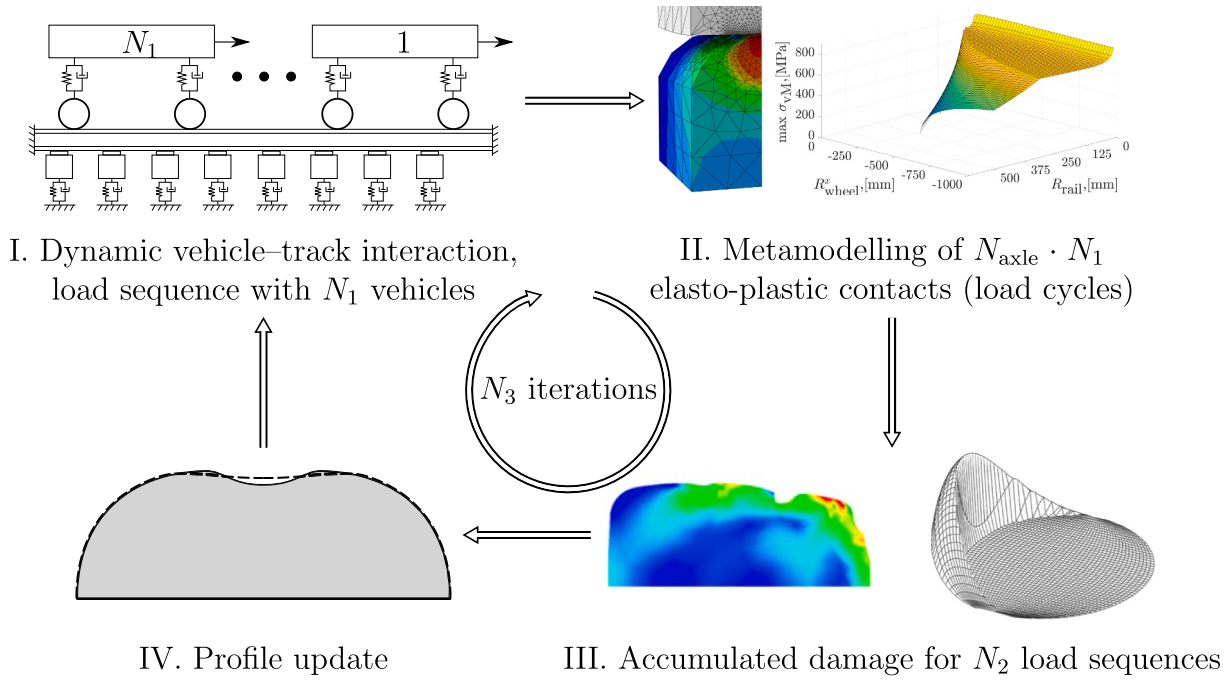

Fig. 6. Illustration of iterative simulation methodology.

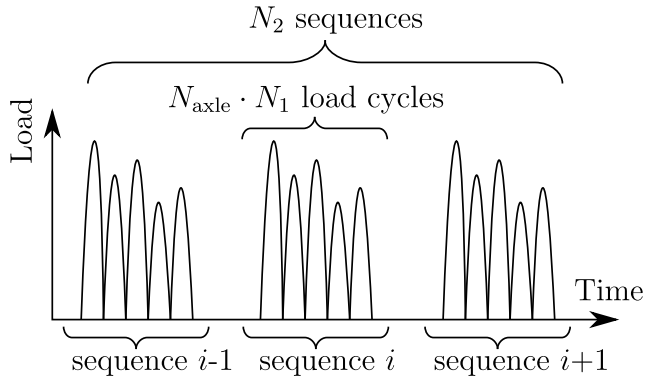

Fig. 7. Illustration of load collective generation based on N_2 identical load sequences, where each load sequence includes $N_{\text{axle}} \cdot N_1$ different load cycles.

of the measured crossing. This is why, it was decided to use a smaller wear ratio $k/H = 8.7 \cdot 10^{-14}$ m^2/N (calibrated to match the average wear rate of 140 mm^3/MGT) to partly compensate for the discrepancy between the materials. Here, k and H are the wear coefficient and hardness used in Archard's wear model.

Due to the fact that it is not computationally feasible to update the rail profiles after each wheel passage, the damage step within the methodology is carried out for $N_{\text{axle}} \cdot N_1 \cdot N_2$ load cycles before updating the dynamics step (i.e. the load environment). Effectively, this means that in the short term it is assumed that the influence of the rail profile degradation on the calculated loads is negligible compared to the influence of various uncertainties in the input data, such as dynamic properties of the track and trains.

4. Representative load sequence – influence of N_1

As described above, N_1 is the number of unique load cases in one load sequence. To generate a load sequence that is representative of the

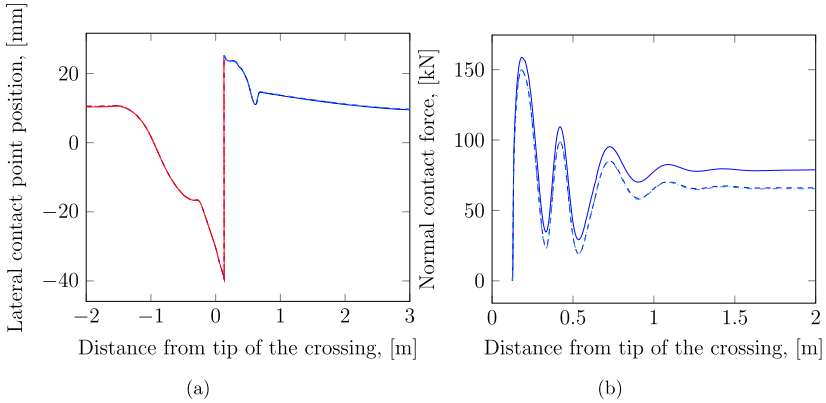

Fig. 8. Comparison of full and reduced vehicle models in terms of time histories of (a) lateral contact point position and (b) normal contact force. Reduced model on wing rail is denoted by ——— and on crossing rail by ——— Front bogie of the full model on wing rail is denoted by – – – and on crossing by – – – while its rear bogie is denoted by –·–·– on wing rail and by –·–·– on crossing rail.

traffic conditions in the investigated railway crossing, accurate information is required about the distributions of traffic types, train speeds, axle loads, wheel–rail friction coefficient, routes and moves, etc. This can be a complicated task. In the current study, the information about traffic conditions is limited. For example, there is no information available about the distribution of train types or the state of the wheel profiles passing the crossing. Here, instead a set containing 250 measured worn wheel profiles from Bombardier Regina passenger trains used in Swedish traffic is applied (see Ref. [22]), while wheel–rail friction coefficient μ and train speed v are assumed to be constant, $\mu = 0.35$ and $v = 90$ km/h, respectively. The axle load is also constant at 19.1 tonnes. The sampling of the wheel profiles is based on their equivalent conicity. Only traffic in through route, facing move is considered.

One of the first questions that arise when creating a representative load sequence is how many unique load cases need to be considered, i.e. the value of N_1. The influence of N_1 on the two types of damage considered in this paper is investigated below.

4.1. Wear

In general it is understood that worn wheel profiles aggravate the wheel–rail dynamic interaction (see e.g. Ref. [23,24]) and lead to a variation in position of the transition point [25]. In particular, wheels with hollow worn wheel profiles may lead to a delayed transition and a higher impact load [24]. Bootstrapping [26] is used to estimate how the sample size of wheel profiles in the load sequence affects the wear simulations. The average wear from a number of reduced samples is compared with the corresponding value from the full sample containing 250 bogies with 250 unique wheel profiles. Fig. 9 presents the predicted wear depth in the cross-section with maximum wear (for the full sample) based on 500 different reduced samples with 125 bogies. The wear depth is normalised by the reference value from the full sample with 250 bogies. Considering the significant uncertainty in traffic load input data, the observed variation of up to 8% suggests that the number of wheel profiles included in the load sequence could possibly be reduced.

4.2. Plastic deformation

A similar analysis has been performed for the simulation of plastic deformation. Fig. 10(a) shows the influence of sample size (250 or 125 bogies with unique wheel profiles) and the order of the bogie passages on the accumulated plastic deformation. The average shape change area from 10 samples with different orders of the 250 wheel profiles was used for the normalisation. Each sampled sequence with 125 wheel profiles was applied twice to match the amount of traffic from the full sample (250 wheel profiles). The results indicate that the order of the bogie passages does not influence the results significantly, but the chosen sample does. For a given reduced sample, the amount of plastic deformation can be underestimated by as much as 30% and, therefore, it is considered preferable to refrain from a reduction in the number of wheel profiles included in the load sequence. In fact, the result of this study means that the number of unique wheel profiles should possibly be higher than the available 250 to generate a representative load sequence.

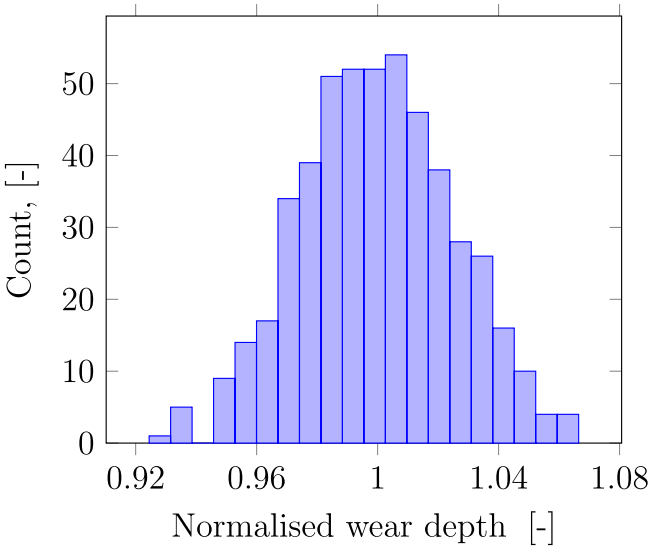

Fig. 9. Histogram (based on 500 samples) of maximum average wear in a critical rail cross-section from 125 bogies with unique wheel profiles (normalised by the reference value from the full sample of 250 bogies).

The influence of material hardening is demonstrated in Fig. 10(b). Here, the case of superposition of independent contributions from 125 bogie passages is compared with the history-dependent case where the work hardening after each load cycle is accounted for. The former case, where the crossing material is virgin for each wheel, leads to a shape change approximately 10 times larger than the latter one, where an accumulation of material hardening is accounted for.

The influence of the individual wheel profile shape on the calculated plastic deformation after one bogie passage over a selected cross-section of the crossing with virgin material is examined in Fig. 11. For the selected cross-section it is observed that about half of the wheel profiles do not cause any plastic deformation. Further, if the magnitudes of the calculated shape change areas from one vehicle (Fig. 11) and 125 vehicles (Fig. 10(b)) are compared, it is estimated that some of the wheels in the studied load sequence are responsible for nearly all of the shape change when they make contact with the virgin material crossing.

5. Frequency of rail profile updating – influence of N_2

Based on the results in Section 4 it is concluded that all available measured wheel profiles need to be retained in the load sequence. The accumulated damage influences the loads generated by the passing wheels. In the short term, i.e. within each iteration, this influence is neglected. The number of load cycles seen by the plasticity calculation within each iteration of the simulation methodology is $N_{\text{axle}} \cdot N_1 \cdot N_2$. In this section, the influence of the number N_2 of repeated identical load sequences contained in one load collective on the calculated rail damage is investigated.

A schematic illustration of the influence of two different values of N_2 on the shape change of a profile is shown in Fig. 12. Fig. 12(a) illustrates the case where the rail profile is updated after the application of load collective 1. Because of the deformation, the new simulation of dynamic vehicle–track interaction results in that the updated load collective 2 is acting on a different part of the profile, expanding the deformed area after two applied load collectives. Fig. 12(b) illustrates the alternative where load collectives 1 and 2 are the same, i.e. the same load collective is applied twice over the same region of the crossing without updating the profile. It can be expected that a more frequent updating of the dynamics (a new iteration in the simulation methodology) would facilitate a larger spread of load positions and, therefore, a smoother and more realistic deformed surface. However, it is believed that the influence of the updating frequency should be declining in the long term.

To verify this, the accumulated plastic strain distribution in a cross-section is compared for two different values of N_2. Fig. 13 presents two cases where the load collective has been updated after each of the 10 load sequences ($N_2 = 1$) or when it has not been updated at all ($N_2 = 10$). The same total number of load cycles has been applied in both examples. It is evident that more plastic strain has been accumulated in the case of $N_2 = 1$ (more frequent updating of the load collective) and the plastic deformation has occurred over a larger area. This outcome matches the illustration in Fig. 12. However, at a later stage of deformation a different situation is observed. Fig. 14 shows similar plots for the same pair of values of N_2, but now the less frequently updated load

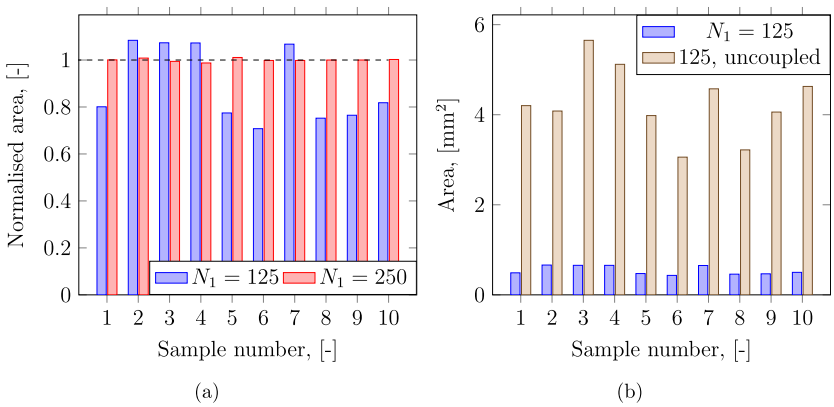

Fig. 10. Comparison of shape change (a) depending on wheel profile sample (N_1) (normalised using the average of 10 samples with $N_1 = 250$), and (b) when accounting or discounting (uncoupled analysis) for material hardening between vehicle passages on the cross-section located 250 mm after the tip of the crossing.

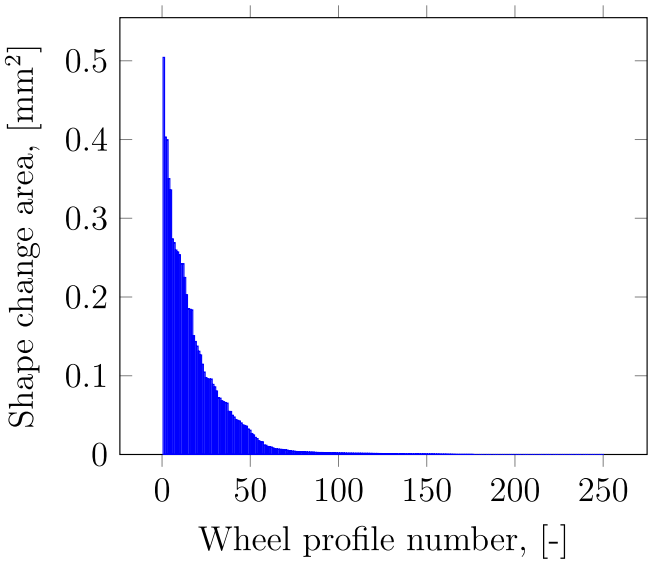

Fig. 11. Independent contributions of each of the 250 wheel profiles (two wheel passages) used in the study of the shape change of the cross-section located 250 mm after the tip of the crossing. Virgin material for all wheel profiles.

collective is updated on 5 occasions, since the total number of applied load sequences has been increased to 50. The maximum accumulated plastic strain is now observed for the case with $N_2 = 10$ but the plastic deformation spans nearly the same area. This outcome suggests that it might not be necessary to update the load collective after every load sequence in a calculation of long-term damage due to material hardening and smaller incremental changes.

The influence of the frequency of updating on the vehicle–track dynamics and contact stresses can be better understood by examining changes in the peak normal wheel–rail contact forces and maximum von Mises stresses for different values of N_2. These are depicted in Fig. 15 for the cross-section located 250 mm after the tip of the crossing. First, it can be noticed that a less frequent updating of dynamics leads to an earlier transition for the studied cross-section because of the larger histogram area, which implies larger number of contacts. The data also suggest that a higher value of N_2 increases the range of values for both the normal contact force and the maximum von Mises stress, meaning that the extreme contact conditions are aggravated for the studied cross-section. However, the opposite picture was observed for some of the cross-sections, so these results are not conclusive.

Finally, a parametric study of the long-term accumulated damage for different values of N_2 ($N_1 = 250$) has been performed for the crossing nose. In each simulation, several iterations have been performed to reach the desired accumulated traffic load. Table 2 shows the investigated parameter combinations to reach a traffic load of 0.5 MGT. The table also compares the simulation time on a modern computer cluster using 10 cores of Intel 2650v3 (“haswell”) CPU and 32 GB of RAM.

It was found that plastic deformation is the dominating damage mechanism for the first set of iterations of the performed simulations. This is in agreement with the experience from the field test, see Fig. 4. The shape change area A_u, see Equation (2), is used to quantify the influence of N_2 on the plasticity calculations, see Fig. 16. It is observed that the time history of the area evolution differs depending on the studied cross-section. For instance, Fig. 16(a) shows that most of the shape change for the cross-section at 250 mm from the crossing tip happens within the first 6 MGT, whereas Fig. 16(b) signals that for the cross-section at 400 mm the process continues throughout the simulated amount of traffic. Also, it seems that there is no long-term correlation between the choice of N_2 and the amount of shape change for different cross-sections. However, it seems that the frequency of updating the dynamics becomes less important with increasing amount of simulated traffic. This is why, it can be concluded that $N_2 = 5$ is a reasonable compromise between accuracy and computational cost.

For the considered cross-sections, Fig. 17 shows that the calculated

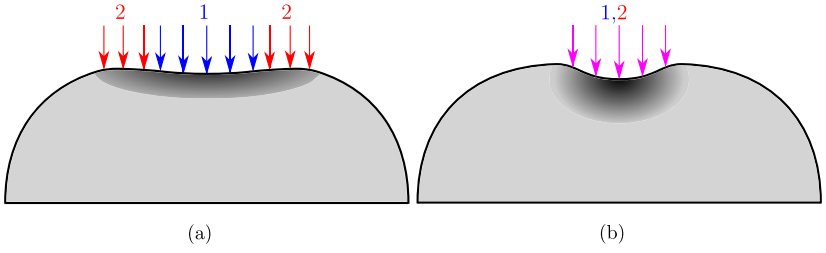

Fig. 12. Illustration of load repositioning for different choices of N_2: (a) $N_2 = 1$ and (b) $N_2 = 2$.

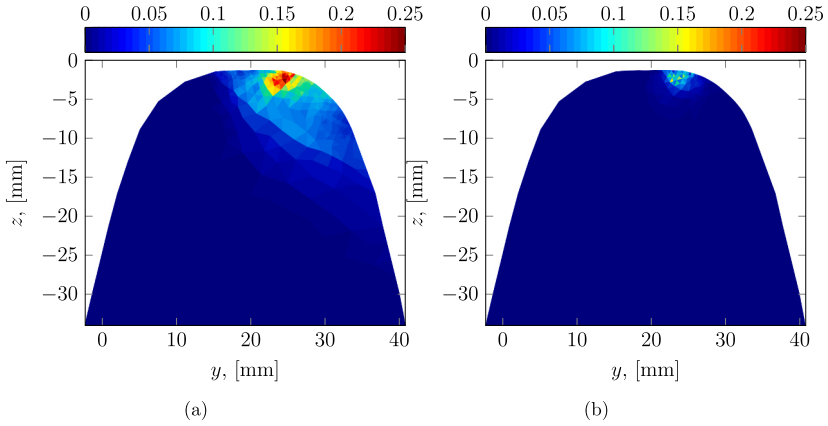

Fig. 13. Comparison of accumulated plastic strain for section 250 after 10 load sequences with $N_1 = 250$ and (a) $N_2 = 1$ (updating of dynamics after each sequence) and (b) $N_2 = 10$ (no updating of dynamics).

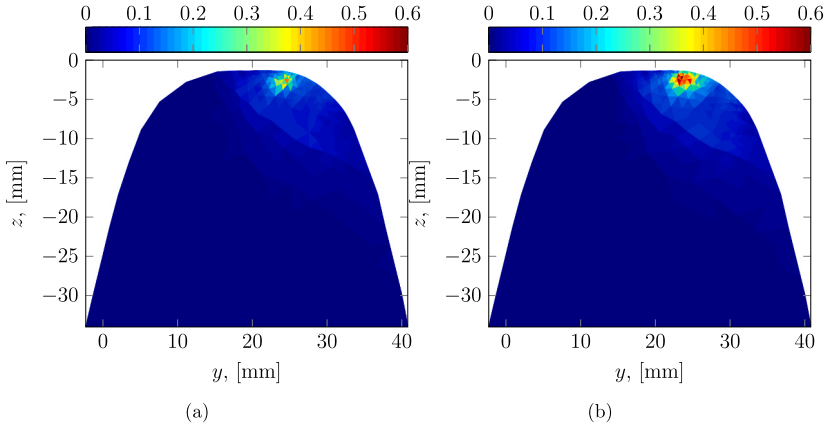

Fig. 14. Comparison of accumulated plastic strain for section 250 after 50 load sequences with $N_1 = 250$ and (a) $N_2 = 1$ (updating of dynamics after each sequence) and (b) $N_2 = 10$ (updating of dynamics after each set of 10 sequences).

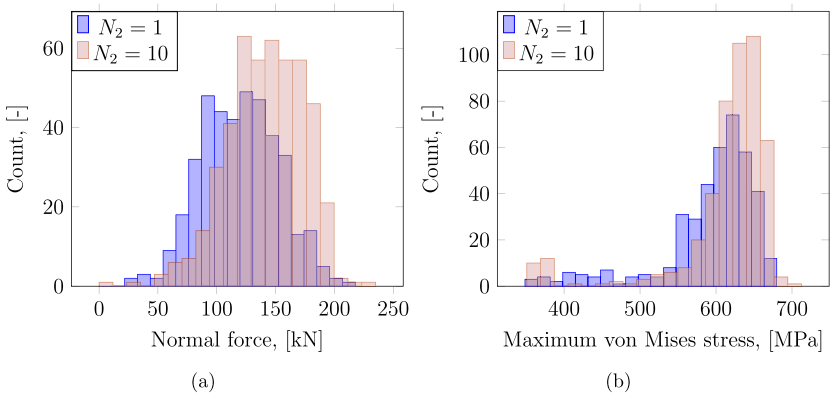

Fig. 15. (a) Comparison of histograms of (a) normal contact force and (b) maximum von Mises stress for section 250 after 50 load sequences with $N_1 = 250$ and $N_2 = 1$ (updating of dynamics after each sequence) and $N_2 = 10$ (updating of dynamics after each set of 10 sequences).

Table 2
Settings for N_2 parameter study to simulate 0.5 MGT of traffic ($\sigma_y = 580$ MPa).

N_1, [−]	N_2, [−]	N_3, [−]	Time, [days]
250	10	5	1.9
250	5	10	2.7
250	2	25	5.2
250	1	50	9.3

increase in wear with increasing traffic load is close to linear, and that the influence of the selection of N_2 is small.

6. Validation

In this section, the predicted rail profile damage after 11.9 MGT for the case with $N_1 = 250$ and $N_2 = 5$ is compared with the corresponding damage measured in the field. Note that only traffic in the through

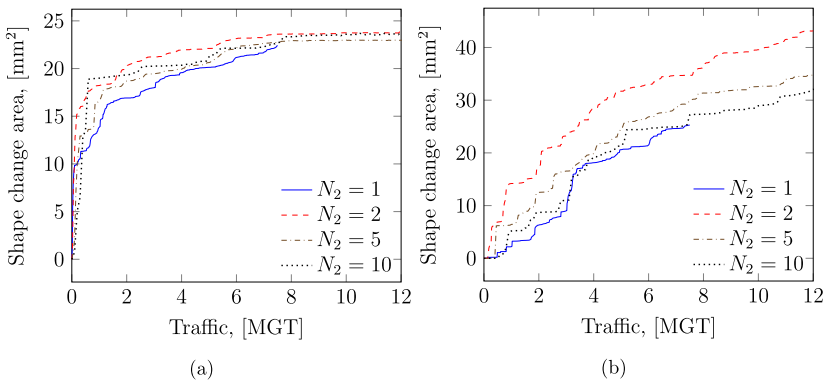

Fig. 16. (a) Comparison of rail profile shape change area for different values of N_2 ($N_1 = 250$) for two cross-sections: (a) 250 mm and (b) 400 mm from the crossing tip. The case $N_2 = 1$ was simulated until 7.5 MGT only.

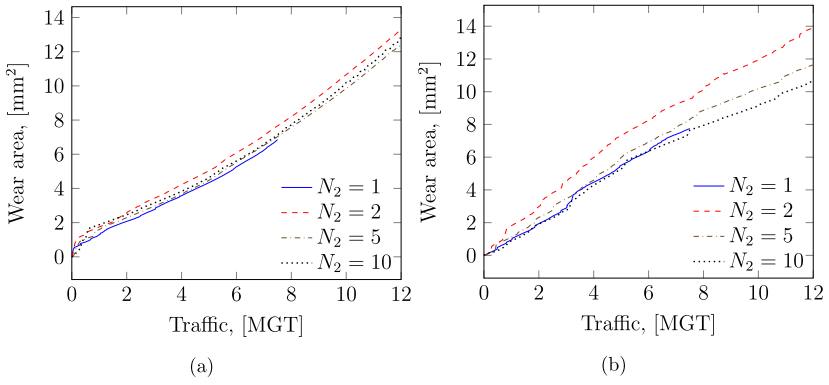

Fig. 17. (a) Comparison of rail profile wear area for different values of N_2 ($N_1 = 250$) for two cross-sections: (a) 250 mm and (b) 400 mm from the crossing tip. The case $N_2 = 1$ was simulated until 7.5 MGT only.

route, facing move has been considered and wing rail damage has been ignored. The results of the simulations are presented in Fig. 18, which correspond to the measurement results shown in Fig. 4. In Fig. 18(a), it is observed that the wear simulations are able to reproduce the three peaks at 250, 400 and 650 mm after the tip present in the measurement data. Although initially the simulated wear rate is considerably lower than the measured one, see Fig. 18(c), the total estimated amount of wear matches rather well the one observed in the field. This is less true for the total amount of simulated profile shape change (plastic deformation), see Fig. 18(b). Despite that the range of values is the same, the simulations overestimate the amount of shape change for almost every cross-section for a given amount of accumulated traffic load. Also, the length of the area affected by the plastic deformation does not grow as much over time, cf. Fig. 4(b). Lastly, the rate of shape change (plastic deformation) predicted by the simulations is much higher in the beginning and localises later on in the narrow region of the crossing between 300 and 450 mm after the tip, see Fig. 18(d), which cannot be supported by the measurement data.

Two measured and predicted rail cross-sections are compared in Fig. 19. It is observed that the simulations overestimate the amount of damage for the cross-section closer to the tip of the crossing, see Fig. 19 (a), while the damage is underestimated for the cross-section further away, see Fig. 19(b). This suggests that many of the wheels used in the current study make the transition too early compared with those that were present at the test site. Furthermore, the information about the distribution of axle loads, which has a significant influence on the magnitude of the impact load, was limited. The observed difference can also be attributed to the employed material model that has been calibrated for hot-rolled manganese steel, due to the absence of test data for EDH manganese steel. However, the predicted rail profiles show good qualitative agreement with the measurements. For a given traffic scenario it is therefore concluded that the methodology can be used as a tool for comparison of different materials used in crossings, as well as for testing of different crossing designs.

The simulation methodology also aids in understanding of how the dynamic loads change with the degradation of the crossing rail. As an example, Fig. 20 presents the distribution of the position for the calculated maximum normal contact force from each bogie passage over the crossing rail. Fig. 20(a) presents a top view of the crossing rail and the distribution of maximum force when the crossing is new. The distribution is confined within a relatively narrow region between 150 and 300 mm after the tip of the crossing. The magnitudes of the forces vary between 150 and 300 kN. Based on the updated rail geometry after 7.5 MGT of traffic, the same distribution has grown in both longitudinal and lateral directions, more than doubling the coverage, see Fig. 20(b). The range of force magnitudes shows the opposite evolution, reducing the upper limit of the contact forces to about 250 kN. Also, the maxima of the peak forces has shifted away from the tip of the crossing. This feature of manganese crossings to adapt to the load environment and reduce the impact forces is also known from field observations.

7. Conclusions

A simulation methodology for the prediction of rail damage has been applied to simulate the long-term plastic deformation and wear in an explosion depth hardened manganese crossing. The multidisciplinary and iterative methodology includes simulations of dynamic vehicle–track interaction in the crossing panel, analyses of wheel–rail normal contact accounting for elasto-plastic material behaviour, and prediction of accumulated damage.

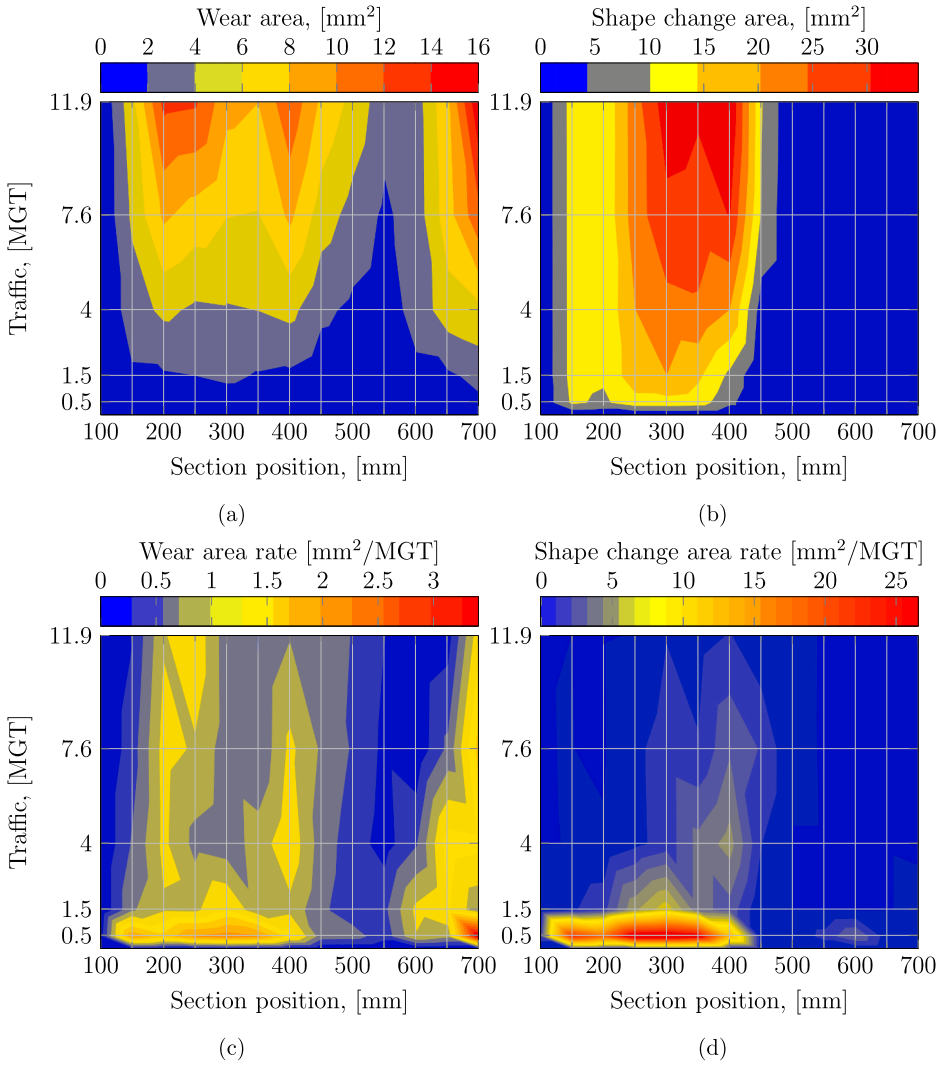

Fig. 18. Simulated data ($N_1 = 250, N_2 = 5$) over time and length of the crossing for different damage measures: (a) wear area [mm^2], (b) shape change area [mm^2], (c) wear area rate [mm^2/MGT] and (d) shape change area rate [mm^2/MGT].

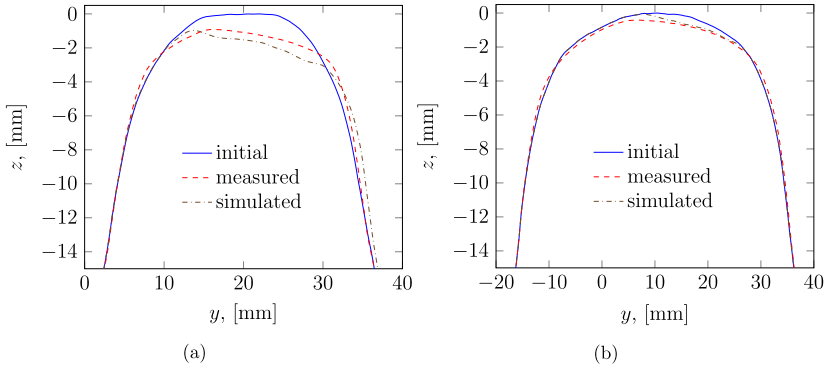

Fig. 19. (a) Comparison of measured profiles and simulated ($N_1 = 250, N_2 = 5$) profiles after 11.9 MGT of traffic load for (a) section 250 mm and (b) section 500 mm from the crossing tip.

To reduce the computational effort, it is shown to be sufficient to reduce the vehicle model to one bogie. The influence of the number of unique wheel profiles included in the load sequence has been addressed. Based on a database containing 250 measured wheel profiles, the results suggest that the number of wheel profiles (N_1) used in the load sequence has a significant influence on the plastic deformation and should be as large as possible to represent the variation in wheel profiles in the field.

Further, the possibility of applying a load collective consisting of several identical load sequences (N_2) instead of updating the rail profiles after each load sequence was explored, since it could further reduce the computational cost. It was concluded that a frequent updating of rail profiles is necessary for a quantitatively realistic prediction of plastic

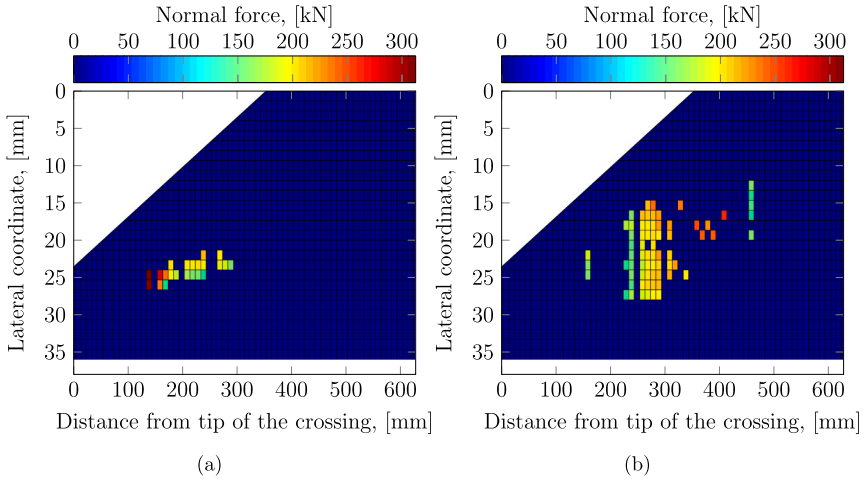

Fig. 20. Simulated distribution ($N_1 = 250, N_2 = 5$) of peak normal contact force on rail cross-sections after (a) 0 MGT and (b) 7.5 MGT of traffic.

deformation. However, over time the rate of plastic deformation is reduced due to work hardening and after a traffic load of about 3 MGT different updating frequencies of the rail profiles yield similar results. In addition, the predicted rate of plastic deformation, using a material model calibrated against experimental data for hot-rolled manganese steel, is close to zero after approximately 11.9 MGT, which opens for the possibility of omitting the expensive calculation of plastic deformation thereafter.

The results from a simulation of the accumulated damage after a traffic load of 11.9 MGT have been compared with in-field measurements. The simulations predicted a higher rate of damage compared with the one measured. This is possibly due to: a) uncertainties present in the input data to the simulations of dynamic vehicle–track interaction (e.g. the distributions of wheel profiles, axle loads, travel routes, etc. are unknown); b) a mismatch between the material used for the calibration of the material model in the FE simulations (hot-rolled manganese steel) and the one present on site (EDH manganese steel); c) not updating the rail profiles after every wheel passage due to unreasonable computational cost. Nevertheless, the methodology shows a good qualitative agreement with measured rail profiles and proves to be a powerful simulation tool for the evaluation of material in railway crossings.

In future work, the possibility of allowing the number of repeated load sequences N_2 to vary from one iteration to the next should be investigated. For example, the value of N_2 could be determined by a maximum allowed change of a profile. It is expected that a low value of N_2 is necessary for the initial iterations, but that higher values can be applied after a certain accumulated traffic load when the rate of plastic deformation is reduced. Further, after a certain number of iterations, it may be possible to omit the calculations of plastic deformation if the rate of plastic deformation becomes negligible compared to the wear rate. This would lead to a significant reduction of computational time.

Notation

Symbol	Meaning
MGT	Million gross tonnes
A_0	Initial area
A	Current area
A_w	Wear area
A_u	Shape change area
$\underline{u}_z$	Vector of vertical surface displacements of rail profile.
N_1	Number of vehicles in a load sequence
N_2	Number of identical load sequences in a load collective.
N_3	Number of iterations of simulation methodology

CRediT authorship contribution statement

Rostyslav Skrypnyk: Methodology, Software, Formal analysis, Writing - original draft, Visualization. **Uwe Ossberger:** Formal analysis, Investigation, Data curation, Visualization. **Björn A. Pålsson:** Conceptualization, Methodology, Writing - review & editing, Supervision. **Magnus Ekh:** Conceptualization, Writing - review & editing, Supervision, Project administration, Funding acquisition. **Jens C.O. Nielsen:** Conceptualization, Software, Writing - review & editing, Supervision, Project administration, Funding acquisition.

Declaration of competing interest

The authors declare that they have no known competing financial interests or personal relationships that could have appeared to influence the work reported in this paper.

Acknowledgements

The current study is part of the on-going activities in CHARMEC – Chalmers Railway Mechanics (www.chalmers.se/charmec). Parts of the study have been funded within the European Union's Horizon 2020 research and innovation programme in the project In2Track2 under grant agreement No 826255. The authors would like to thank voestalpine VAE GmbH and the Swedish Transport Administration (Trafikverket) for their support. The simulations were performed on resources at Chalmers Centre for Computational Science and Engineering (C3SE) provided by the Swedish National Infrastructure for Computing (SNIC).

N_{axle}	Number of axles in a bogie
k	Dimensionless wear coefficient
H	Material hardness

References

[1] Y. Bezin, M.L. Sarmiento-Carnevali, M. Sichani, S. Neves, D. Kostovasilis, S. D. Bemment, T.J. Harrison, C.P. Ward, R. Dixon, Dynamic Analysis and Performance of a Repoint Track Switch, Veh. Syst. Dyn. (2019) 1–21, https://doi.org/10.1080/00423114.2019.1612925.

[2] J.H. Sällström, T. Dahlberg, M. Ekh, J.C.O. Nielsen, Research report, in: State-of-the Art Study on Railway Turnouts – Dynamics and Damage, vol. 8, Department of Applied Mechanics, Chalmers University of Technology, Gothenburg, Sweden, 2004, p. 50, 2004.

[3] E. Kassa, J.C.O. Nielsen, Dynamic interaction between train and railway turnout: full-scale field test and validation of simulation models, Veh. Syst. Dyn. 46 (sup1) (2008) 521–534, https://doi.org/10.1080/00423110801993144.

[4] B.A. Pålsson, Optimisation of railway crossing geometry considering a representative set of wheel profiles, Veh. Syst. Dyn. 53 (2) (2015) 274–301, https://doi.org/10.1080/00423114.2014.998242.

[5] X. Li, P.T. Torstensson, J.C.O. Nielsen, Simulation of vertical dynamic vehicle–track interaction in a railway crossing using Green's functions, J. Sound Vib. 410 (2017) 318–329, https://doi.org/10.1016/j.jsv.2017.08.037.

[6] A. Johansson, B.A. Pålsson, M. Ekh, J.C.O. Nielsen, M.K.A. Ander, J. Brouzoulis, E. Kassa, Simulation of wheel–rail contact and damage in switches & crossings, Wear 271 (1–2) (2011) 472–481, https://doi.org/10.1016/j.wear.2010.10.014.

[7] D. Nicklisch, J.C.O. Nielsen, M. Ekh, A. Johansson, B.A. Pålsson, A. Zoll, J. Reinecke, Simulation of wheel-rail contact and subsequent material degradation in switches & crossings, in: Proceedings 21st International Symposium on Dynamics of Vehicles on Roads and Tracks, 2009, pp. 1–14. Stockholm, Sweden, (available on CD).

[8] M. Pletz, W. Daves, H. Ossberger, A wheel passing a crossing nose: dynamic analysis under high axle loads using finite element modelling, Proc. Inst. Mech. Eng. - Part F J. Rail Rapid Transit 226 (6) (2012) 603–611, https://doi.org/10.1177/0954409712448038.

[9] Z. Wei, C. Shen, Z. Li, R. Dollevoet, Wheel–rail impact at crossings: relating dynamic frictional contact to degradation, J. Comput. Nonlinear Dynam. 12 (4) (2017), 041016, https://doi.org/10.1115/1.4035823.

[10] R. Lewis, U. Olofsson, Chapter: Basic Tribology of the Wheel-Rail Contact, Wheel-Rail Interface Handbook, Woodhead Publishing Limited, Cambridge, 2009, pp. 34–57.

[11] M. Wiest, E. Kassa, W. Daves, J.C.O. Nielsen, H. Ossberger, Assessment of methods for calculating contact pressure in wheel-rail/switch contact, Wear 265 (9) (2008) 1439–1445, https://doi.org/10.1016/j.wear.2008.02.039.

[12] R. Skrypnyk, J.C.O. Nielsen, M. Ekh, B.A. Pålsson, Metamodelling of wheel–rail normal contact in railway crossings with elasto-plastic material behaviour, Eng. Comput. 35 (1) (2019) 139–155, https://doi.org/10.1007/s00366-018-0589-3.

[13] R. Skrypnyk, M. Ekh, J.C.O. Nielsen, B.A. Pålsson, Prediction of plastic deformation and wear in railway crossings – comparing the performance of two rail steel grades, Wear 428–429 (2019) 302–314, https://doi.org/10.1016/j.wear.2019.03.019.

[14] S. Iwnicki, Manchester benchmarks for rail vehicle simulation, Veh. Syst. Dyn. 30 (3–4) (1998) 295–313, https://doi.org/10.1080/00423119808969454.

[15] J.J. Kalker, A fast algorithm for the simplified theory of rolling contact, Veh. Syst. Dyn. 11 (1) (1982) 1–13, https://doi.org/10.1080/00423118208968684.

[16] J.C.O. Nielsen, R. Lundén, A. Johansson, T. Vernersson, Train-track interaction and mechanisms of irregular wear on wheel and rail surfaces, Veh. Syst. Dyn. 40 (1–3) (2003) 3–54, https://doi.org/10.1076/vesd.40.1.3.15874.

[17] B.A. Pålsson, J.C.O. Nielsen, Dynamic vehicle–track interaction in switches and crossings and the influence of rail pad stiffness – field measurements and validation of a simulation model, Veh. Syst. Dyn. 53 (6) (2015) 734–755, https://doi.org/10.1080/00423114.2015.1012213.

[18] A. Olsson, G. Sandberg, O. Dahlblom, On Latin hypercube sampling for structural reliability analysis, Struct. Saf. 25 (1) (2003) 47–68, https://doi.org/10.1016/S0167-4730(02)00039-5.

[19] N. Ohno, J.-D. Wang, Kinematic hardening rules with critical state of dynamic recovery, part I: formulation and basic features for ratchetting behavior, Int. J. Plast. 9 (3) (1993) 375–390, https://doi.org/10.1016/0749-6419(93)90042-O.

[20] J.F. Archard, Contact and rubbing of flat surfaces, J. Appl. Phys. 24 (8) (1953) 981–988, https://doi.org/10.1063/1.1721448.

[21] T. Jendel, Prediction of wheel profile wear – comparisons with field measurements, Wear 253 (1) (2002) 89–99, https://doi.org/10.1016/S0043-1648(02)00087-X.

[22] B.A. Pålsson, J.C.O. Nielsen, Track gauge optimisation of railway switches using a genetic algorithm, Veh. Syst. Dyn. 50 (sup1) (2012) 365–387, https://doi.org/10.1080/00423114.2012.665167.

[23] K. Sawley, H. Wu, The formation of hollow-worn wheels and their effect on wheel/rail interaction, Wear 258 (7–8) (2005) 1179–1186, https://doi.org/10.1016/j.wear.2004.03.029.

[24] B.A. Pålsson, J.C.O. Nielsen, Wheel–rail interaction and damage in switches and crossings, Veh. Syst. Dyn. 50 (1) (2012) 43–58, https://doi.org/10.1080/00423114.2011.560673.

[25] J. Wiedorn, W. Daves, U. Ossberger, H. Ossberger, M. Pletz, Simplified explicit finite element model for the impact of a wheel on a crossing – validation and parameter study, Tribol. Int. 111 (2017) 254–264, https://doi.org/10.1016/j.triboint.2017.03.023.

[26] H. Varian, Bootstrap tutorial, Math. J. 9 (4) (2005) 768–775.